

Glitch in the Matrix: A Large Scale Benchmark for Content Driven Audio-Visual Forgery Detection and Localization

Zhixi Cai¹, Shreya Ghosh², Abhinav Dhall³, Tom Gedeon², Kalin Stefanov¹, Munawar Hayat¹

¹Monash University, ² Curtin University, ³ Indian Institute of Technology Ropar,

{zhixi.cai, kalin.stefanov, munawar.hayat}@monash.edu,

{shreya.ghosh, tom.gedeon}@curtin.edu.au, abhinav@iitrpr.ac.in

Abstract

Most deepfake detection methods focus on detecting spatial and/or spatio-temporal changes in facial attributes and are centered around the binary classification task of detecting whether a video is real or fake. This is because available benchmark datasets contain mostly visual-only modifications present in the entirety of the video. However, a sophisticated deepfake may include small segments of audio or audio-visual manipulations that can completely change the meaning of the video content. To address this gap, we propose and benchmark a new dataset, Localized Audio Visual DeepFake (LAV-DF), consisting of strategic content-driven audio, visual and audio-visual manipulations. The proposed baseline method, Boundary Aware Temporal Forgery Detection (BA-TFD), is a 3D Convolutional Neural Network-based architecture which effectively captures multimodal manipulations. We further improve (i.e. BA-TFD+) the baseline method by replacing the backbone with a Multiscale Vision Transformer and guide the training process with contrastive, frame classification, boundary matching and multimodal boundary matching loss functions. The quantitative analysis demonstrates the superiority of BA-TFD+ on temporal forgery localization and deepfake detection tasks using several benchmark datasets including our newly proposed dataset. The dataset, models and code are available at <https://github.com/ControlNet/LAV-DF>.

1. Introduction

¹Increasingly powerful deep learning algorithms (e.g. Autoencoders [77] and Generative Adversarial Networks [33]) accompanied by the rapid advances in computing power have enabled the generation of highly realistic synthetic media commonly referred to as *deepfakes*².

¹The paper is under consideration/review at Computer Vision and Image Understanding Journal.

²In the text, *deepfake* and *forgery* are used interchangeably.

Audio-visual deepfake content generation utilizes methods for voice cloning [42, 91], face reenactment [73, 89], and face swapping [50, 70].

Audio-visual deepfakes include videos that have been either manipulated or created from scratch to primarily mislead, deceive or influence audiences. Given that access to deepfake generation technologies has become widespread and the technologies are easy to use, some researchers argue that deepfakes are “threat to democracy” [8, 78, 80, 88]. For example, [87] used a video of the former United States president Barack Obama to demonstrate a novel face reenactment method. In the resultant realistic video, the former president’s lip movement is synchronized with the speech of another person. This type of manipulations has the potential to mislead people in forming wrong opinions and could have serious consequences.

Given the rapid grow of fake videos on the Internet, robust and accurate deepfake detection methods are increasingly important. This triggered the release of several benchmark datasets for deepfake detection [26, 37, 49, 76] and state-of-the-art deepfake detection methods [4, 15, 23, 40, 53, 75, 97] demonstrate promising performance on those benchmark datasets, which define the problem as a binary classification task (i.e. classify the whole input video as *real* or *fake*).

Fake content however, may only constitute a small part(s) of a long real video [19] and these modified segment(s) could completely change the meaning and sentiment of the original content. Lets consider the example illustrated in Figure 1, where the real video on the left captures the person saying “Vaccinations are safe”. When the word “safe” is replaced with its antonym “dangerous”, the meaning and sentiment of the video is significantly changed. This type of video forgeries can effectively manipulate the public opinion, particularly when targeting media involving famous individuals, as the example with Barack Obama. Given the underlying assumption (i.e. deepfake detection is a binary classification problem) of the current deepfake detection benchmark datasets and meth-

ods, it is possible that the state-of-the-art techniques may not perform well in identifying this new type of manipulations.

This paper addresses the important task of content-driven forgery localization and detection in video. In terms of benchmark datasets, there is a significant gap in the availability of datasets for multimodal content-driven forgery localization and detection. This paper proposes a pipeline for generating such large-scale dataset that can serve as a valuable resource for future research in this area. Furthermore, this paper also introduces a novel multimodal method that utilizes audio and visual information to precisely detect the boundaries of fake segments in videos. The **main contributions** of our work are,

- A large-scale public dataset, *Localized Audio Visual DeepFake*, for temporal forgery localization and detection.
- A multimodal method, *Boundary Aware Temporal Forgery Detection Plus*, for fake segment localization and detection.
- A thorough validation of the method’s components and comprehensive comparison with the state-of-the-art.

2. Related Work

This section reviews the relevant literature on deepfake detection datasets and methods. Given the similarities between temporal forgery localization and temporal action localization, previous work in the latter area is also reviewed.

2.1. Deepfake Detection Datasets

Deepfake detection research is driven by datasets generated with various deepfake generation approaches. We present a summary of the deepfake detection datasets available to the research community in Table 1. The first deepfake dataset named DF-TIMIT was proposed by [49]. DF-TIMIT curation process involved face swapping on VidTimit dataset [79]. Later, UADFV [94], FaceForensics++ [76] and Google DFD [69] were introduced, and FaceForensics++ has become a popular benchmark dataset for multiple deepfake detection methods [74,90]. The main limitation of the aforementioned datasets is their size (i.e. a maximum of thousands of video samples). Given that CNNs and Transformers (commonly used for deepfake detection) are data-demanding techniques, these datasets have low generalization capability [56]. In 2020, Facebook (i.e. Meta) published the large-scale dataset DFDC [26] for deepfake detection with more than 100K samples. Until today, DFDC is the standard benchmark used for deepfake detection methods [15,96]. After DFDC, several datasets



Figure 1. **Content-driven audio-visual manipulation.** In the real video (left) the subject is saying “Vaccinations are safe”. In the audio-visual deepfake (right) created from the real video, “safe” is changed to “dangerous” (resulting in a significant change in perceived sentiment). The green-edge frames are real and red-edge are fake. *Note that through a subtle audio-visual manipulation, the meaning of the video content has been completely changed.*

targeting different specializations were introduced. For example, WildDeepfake [106] for web-crawled in-the-wild fake video detection, FFIW_{10K} [103] for detecting fake faces in videos containing multiple faces, KoDF [51] for Korean deepfake detection, and DF-Platter [66] for detecting multi-face heterogeneous deepfakes. DeeperForensics [43] is another notable dataset that overcomes the bias of having high number of fake videos. However, all those datasets mainly consider visual-only deepfake detection. In 2021, FakeAVCeleb [47] was introduced including both face swapping and audio-based face reenactment. This dataset includes fake audio generated from SV2TTS [42], which makes it the first deepfake detection dataset focusing on audio-visual manipulations.

Given that all of the those datasets regard the deepfake detection as a binary classification problem, ForgeryNet [37] dataset was introduced, which includes visual-only face swapping in random frames and is suitable for both video/image classification and spatial/temporal forgery localization. However, ForgeryNet only applies random face swapping in the visual modality and does not consider audio and content-driven modifications. To bridge this gap, we propose a multimodal content-driven temporal forgery localization and detection dataset.

2.2. Deepfake Detection Methods

Deepfake detection methods can be categorized into two categories: traditional machine learning and deep learning approaches. The traditional machine learning methods include EM [35] and SVM [97]. On the other hand, deep learning methods include CNN [25], RNN [15,65] and ViT [22,38,92]. Most of the prior deepfake detection methods focus on temporal inconsistencies [34,52] and multimodal synchronization [19,64,90,105] to detect fake videos.

All of the above mentioned methods employ classification centric approach. Thus, those methods do not have temporal localization capabilities. Only MDS [19] demonstrated scenarios where only parts of the video are modified,

Table 1. **Details for publicly available deepfake datasets in a chronologically ascending order.** The LAV-DF dataset details are reported in the last row. *Cl*: Classification, *SL*: Spatial Localization, *TFL*: Temporal Forgery Localization, *FS*: Face Swapping, and *RE*: ReEnactment.

Dataset	Year	Tasks	Manipulated Modality	Manipulation Method	#Subjects	#Real	#Fake	#Total
DF-TIMIT [49]	2018	Cl	V	FS	43	320	640	960
UADFV [97]	2019	Cl	V	FS	49	49	49	98
FaceForensics++ [76]	2019	Cl	V	FS/RE	-	1,000	4,000	5,000
Google DFD [69]	2019	Cl	V	FS	-	363	3,068	3,431
DFDC [26]	2020	Cl	AV	FS	960	23,654	104,500	128,154
DeeperForensics [43]	2020	Cl	V	FS	100	50,000	10,000	60,000
Celeb-DF [56]	2020	Cl	V	FS	59	590	5,639	6,229
WildDeepfake [106]	2020	Cl	-	-	-	3,805	3,509	7,314
FFIW _{10K} [103]	2021	Cl	V	FS	-	10,000	10,000	20,000
KoDF [51]	2021	Cl	V	FS/RE	403	62,166	175,776	237,942
FakeAVCeleb [47]	2021	Cl	AV	RE	600+	570	25,000+	25,500+
ForgeryNet [37]	2021	SL/TFL/Cl	V	Random FS/RE	5,400+	99,630	121,617	221,247
DF-Platter [66]	2023	Cl	V	FS	454	133,260	132,496	265,756
LAV-DF (ours)	2022	TFL/Cl	AV	Content-driven RE	153	36,431	99,873	136,304

although this approach is primarily designed for classification. Our dataset and method are designed to consider both audio-visual deepfake detection and temporal localization.

2.3. Temporal Action Localization

Since the temporal forgery localization task is similar to temporal action localization, we also review the literature in this domain. For temporal action localization, ActivityNet [10], THUMOS14 [39], HACS [100], EPIC-KITCHEN [24], and FineAction [63] are popular benchmark datasets. Temporal action localization methods can be classified as two types: 2-stage approaches [61, 93, 98], where the temporal bounding box proposals are generated at first and then are classified as different classes, and 1-stage approaches [9, 58, 60, 62, 67, 82, 95, 99], which directly predict the final temporal segments.

For temporal forgery localization, there is no requirement to classify the foreground segments, in other words, the background is always real and the foreground is always fake. Hence, 1-stage temporal action localization approaches are more relevant for the task. According to [3], these approaches can be grouped in two main categories: methods based on anchors and methods based on predicting the boundary probabilities. Anchor-based methods [31, 32, 84, 85] utilize sliding windows in the video to detect segments. [59] proposed a new framework to generate proposals that predicts the boundary probabilities based on start and end timestamps. This approach can access the global context information to generate more precise and flexible segment proposals than anchor-based methods. Based on this method, several other approaches were proposed to enhance performance [57, 86].

All temporal action localization methods described above are visual-only, which is not optimal for the task of

temporal forgery localization. The importance of accessing the multimodal information for temporal action localization was recently raised by [3].

2.4. Proposed Multimodal Approach

This paper proposes a multimodal method for precise boundary proposal estimation to detect and localize fake segments videos. We quantitatively compare the performance of the proposed method with existing state-of-the-art approaches, including BMN [57], AGT [67], MDS [19], AVFusion [3], BSN++ [86], TadTR [62], ActionFormer [99], and TriDet [82].

3. Localized Audio Visual DeepFake Dataset

We created a large-scale audio-visual deepfake dataset containing 136,304 videos (36,431 real and 99,873 fake). Our data generation pipeline is illustrated in Figure 2. The generation is guided by relevant words in the video transcripts and specifically, the manipulation strategy is to replace strategic words with their antonyms, which leads to a significant change in the perceived sentiment of the statement.

3.1. Audio-Visual Data Sourcing

The real videos in this dataset are collected from the VoxCeleb2 dataset [20], which is a large-scale facial video dataset containing more than 1 million utterance videos of 6,112 speakers. To ensure consistency, the faces within these videos are tracked and cropped using the Dlib facial detector [48] at 224×224 resolution. The VoxCeleb2 dataset offers a diverse range of video lengths, spoken languages, and voice qualities. Our dataset includes only English-speaking videos, where the spoken language was

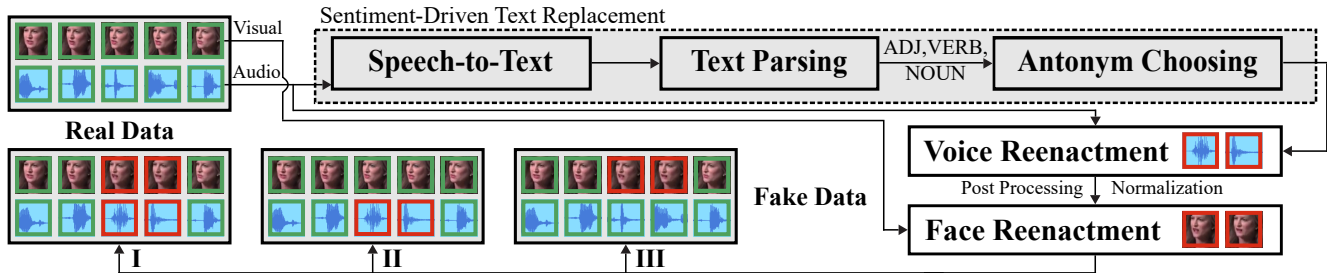


Figure 2. **Content-driven audio-visual manipulation for the creation of the LAV-DF dataset.** The real transcript is used to find the word tokens for replacement based on the largest change in perceived sentiment. Then the modified tokens are used as input for generating audio. Post-processing and normalization are applied to the generated audio to maintain loudness consistency in the temporal neighborhood. The generated audio is then used as input for facial reenactment. The green-edge audio and visual frames are real data, and red-edge are fake data. *In total, three categories of data are generated: Fake Audio and Fake Visual, Fake Audio and Real Visual and Real Audio and Fake Visual.*

detected through the confidence score generated by the Google Speech-to-Text service³. We leveraged the same service to generate the transcripts.

3.2. Audio-Visual Data Generation

After sourcing the real videos, the next step is to analyze each video transcript for content-driven deepfake generation. The generation process includes transcript manipulation, followed by generation of the corresponding audio and visual modalities.

3.2.1 Transcript Manipulation

Following the collection and wrangling of the real data, the next step is to analyze the transcript of a video denoted as $D = \{d_0, d_1, \dots, d_m, \dots, d_n\}$, where d_i represents individual word tokens and n denotes the total number of tokens in the transcript. The objective is to identify the tokens within D that should be replaced in order to achieve the maximum change in perceived sentiment. This process aims to create a modified transcript $D' = \{d_0, d_1, \dots, d'_m, \dots, d_n\}$, which consists of most of the original tokens from D and the replacements for a few specific tokens. The replacement tokens, denoted as d' , are selected from a set \hat{d} containing antonyms of d , sourced from WordNet [30]. To determine the sentiment value of the transcript, we employed the sentiment analyzer available in NLTK [5]. Specifically, for each token d in a transcript D , the replacement is found with,

$$\tau = \operatorname{argmax}_{d \in D, d' \in \hat{d}} |S(D) - S(D')|$$

Then all replacements in a transcript D are found as follows,

$$\theta = \operatorname{argmax}_{\{\tau_m\}_{m=1}^M} \left| \sum_{i=1}^M \Delta S(\tau_i) \right|$$

³<https://cloud.google.com/speech-to-text>

where $\Delta S(\tau_i)$ is the difference in sentiment score of the original and modified transcripts when utilizing the replacement τ_i and M is the maximum number of replacements.

There is up to 1 replacement for videos shorter than 10 seconds; otherwise, there can be a maximum of 2 replacements. The shift in sentiment distribution following the manipulations is visualized in Figure 3 (a), while the histogram of $|\Delta S|$ indicating that the sentiment of most transcripts has been successfully changed, is shown in Figure 3 (b).

3.2.2 Audio Generation

After the transcript manipulation, the next step is to generate speaker-specific audio for the replacement tokens. Motivated by the prior work on adaptive text-to-speech methods [14, 42, 68], we adopted SV2TTS [42] for speaker-specific audio generation. SV2TTS consists of three modules: 1) An encoder module responsible for extracting the style embedding of the reference speaker, 2) A spectrogram generation module based on Tacotron 2 [81] utilizing replacement tokens and the speaker style embedding, and 3) A vocoder module based on WaveNet [71], which generates realistic audio using the spectrogram. In the audio generation, we utilized a pre-trained SV2TTS model to generate the audio segments. Then, we performed loudness normalization on the generated audio segments by considering the corresponding real audio neighbors. The rationale behind the loudness normalization is to generate a more realistic counterpart of the audio segment chosen for replacement.

3.2.3 Video Generation

The generated audio is used as input for generating the corresponding visual frames. Wav2Lip [73] facial reenactment is used for this task, as it has been shown to achieve state-of-the-art output generation quality along with better generalization [41, 44]. We encountered several issues with us-

ing other popular visual generation methods such as AD-NeRF [36] and ATVGnet [17]. For example, AD-NeRF does not fit in our generation context (*i.e.* zero-shot generation of unseen speakers), and ATVGnet uses a static reference image as input for facial reenactment, resulting in pose inconsistencies on the boundaries between real and fake segments. In contrast, Wav2Lip uses a reference video and target audio as input and generates an output video in which the person in the reference video lip-syncs to the target audio content, ensuring pose consistency between real and fake segments. We employed a pre-trained Wav2Lip model and upscaled the generated visual segments to a resolution of 224×224 . The generated audio-visual segments are then synchronized and used to replace the original audio-visual segments.

Similar to [46], LAV-DF includes three categories of generated data,

- **Fake Audio and Fake Visual.** Both the real audio and visual segments corresponding to the replacement tokens are manipulated.
- **Fake Audio and Real Visual.** Only the real audio segments corresponding to the replacement tokens are manipulated. To keep the fake audio and real visual segments synchronized, the corresponding real visual segments are length-normalized.
- **Real Audio and Fake Visual.** Only the real visual segments corresponding to the replacement tokens are manipulated and the length of the fake visual segments is normalized to match the length of the real audio segments.

3.3. Dataset Statistics

The dataset contains 136,304 videos of 153 unique identities, with 36,431 real videos and 99,873 videos containing fake segments. For benchmarking, we splitted the dataset into 3 identity-independent subsets: train (78,703 videos of 91 identities), validation (31,501 videos of 31 identities), and test (26,100 videos of 31 identities). Summary of main statistics of the dataset is presented in Figure 3.

The dataset includes a total of 114,253 fake segments, with duration $(0, 1.6]$ seconds and an average length of 0.65 seconds. Notably, 89.26% of the fake segments are shorter than 1 second. The maximum length of the videos in the dataset is 20 seconds and 69.61% of the videos are shorter than 10 seconds. In terms of modality modification, the distribution is balanced among the four types: visual-modified, audio-modified, both-modified and real. Additionally, the majority of the videos (62.72%) contain only 1 fake segment, while a smaller proportion of videos (10.55%) include 2 fake segments.

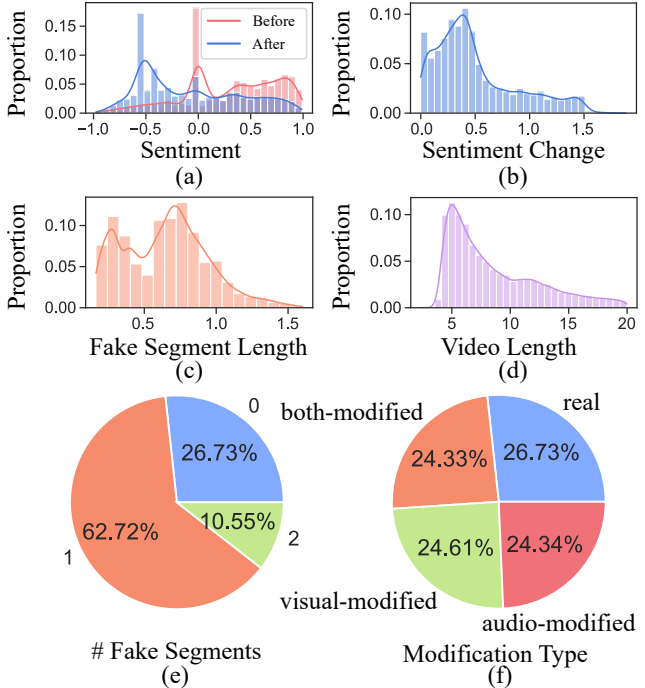


Figure 3. **Statistics of the LAV-DF dataset.** (a) Distribution of sentiment scores before and after content-driven deepfake generation, (b) Histogram of sentiment changes $|\Delta S|$, (c) Distribution of fake segment lengths, (d) Distribution of video lengths, (e) Proportion of number of fake segments, and (f) Proportion of modifications.

3.4. Dataset Quality

Table 2 provides a quantitative comparison (PSNR and SSIM) with existing dataset generation pipelines in terms of visual quality, demonstrating that our pipeline achieves better visual quality on the VoxCeleb2 dataset.

Table 2. **Visual quality of the LAV-DF dataset.** We maintained the experimental protocol and adopted the scores on VoxCeleb2 for the related deepfake generation pipelines from [102].

Method	PSNR	SSIM
ATVGnet [17]	29.41	0.826
Wav2Lip [73]	29.54	0.846
MakeitTalk [104]	29.51	0.817
Rhythmic Head [16]	29.55	0.779
PC-AVS [102]	29.68	0.886
LAV-DF (Ours)	33.06	0.898

4. Boundary Aware Temporal Forgery Detection+ Method

The objective is to detect and localize multimodal manipulations given an input video. To this end, we designed the proposed method BA-TFD+ in such a way that it has the capability to capture deepfake artifacts and localize the boundary of fake segments. An overview of the proposed method is depicted in Figure 4 and Algorithm 1.

4.1. Preliminaries

The training dataset $\mathbb{D} \supset \{X_i, Y_i\}_{i=1}^n$ comprises of n multimodal inputs X_i with visual modality V_i and audio modality A_i , and the associated output labels Y_i . The proposed model BA-TFD+ with trainable parameters θ is optimized to map the inputs X_i to the outputs Y_i . Each X_i has a different number of frames t_i . In order to simplify the batch training of the model, we padded the temporal axis for all X_i to T .

4.2. Visual Encoder

The goal of the visual encoder $\mathcal{F}_{\mathcal{E}_v}$ is to capture the frame-level spatio-temporal features from the input visual modality $V \supset \{V_i\}_{i=1}^n$ using an MViTv2 [55]. MViTv2 achieves seminal performance gain for different video analysis tasks including video action recognition and detection. In addition, MViTv2 leverages hierarchical multi-scale features compared to the basic ViT [27]. Our backbone MViTv2-Base model comprises of 4 blocks and 24 multi-head self-attention layers. As illustrated in Figure 4, the visual encoder $\mathcal{F}_{\mathcal{E}_v}$ maps the inputs $V \in \mathbb{R}^{C \times T \times H \times W}$ (T is the number of frames, C is the number of channels, and H and W are the height and width of the frames) to latent space $\mathbf{z}_v \in \mathbb{R}^{C_f \times T}$ (C_f is the dimension of the features).

4.3. Audio Encoder

The goal of the ViT-based [27] audio encoder $\mathcal{F}_{\mathcal{E}_a}$ is to learn meaningful features from the raw input audio modality $A \supset \{A_i\}_{i=1}^n$. Following previous work [40, 96], we pre-process the raw audio A to generate representative mel-spectrograms $A' \in \mathbb{R}^{F_m \times T_a}$ ($T_a = \tau T$ is the temporal dimension and $\tau \in \mathbb{N}^*$, \mathbb{N}^* denotes positive integers, and F_m is the length of the mel-frequency cepstrum features). In order to keep the audio-visual synchronization, we reshape the temporal axis of the mel-spectrograms to $\tau F_m \times T$. The reshaped spectrograms A' are given as input to the ViT blocks of the audio encoder $\mathcal{F}_{\mathcal{E}_a}$ ⁴. The audio encoder $\mathcal{F}_{\mathcal{E}_a}$ maps the mel-spectrograms A' to the latent space $\mathbf{z}_a \in \mathbb{R}^{C_f \times T}$, where C_f is the features dimension.

⁴We only incorporate the multi-head self-attention layers of the ViT for the audio encoder.

Algorithm 1: Training procedure of BA-TFD+

Data: Training data $\mathbb{D} \supset \{X_i, Y_i\}_{i=1}^n$, Modality modification flag $\mathbb{E} = \{\eta_i = (\eta_{vi}, \eta_{ai})\}_{i=1}^n$, Weights of losses λ

Result: Parameters of the model θ

$\theta \leftarrow$ Initialize the parameters randomly;

$Y_0 \leftarrow$ label for real data;

while θ not converged **do**

$(V, A, Y) \leftarrow$ Next sample from \mathbb{D} ;

$(\eta_v, \eta_a) \leftarrow$ Next flag from \mathbb{E} ;

$Y_v \leftarrow$ if η_v then Y else Y_0 ;

$Y_a \leftarrow$ if η_a then Y else Y_0 ;

$Y^{(b)} \leftarrow$ Generate labels from Y ;

$(Y_v^{(b)}, Y_v^{(f)}) \leftarrow$ Generate labels from Y_v ;

$(Y_a^{(b)}, Y_a^{(f)}) \leftarrow$ Generate labels from Y_a ;

$\mathbf{z}_v \leftarrow \mathcal{F}_{\mathcal{E}_v}(V)$;

$\mathbf{z}_a \leftarrow \mathcal{F}_{\mathcal{E}_a}(\text{mel-spectrogram}(A))$;

$Y^{(c)} \leftarrow \eta_{vi} \wedge \eta_{ai}$;

$\mathcal{L}_c \leftarrow \text{ContrastiveLoss}(\mathbf{z}_v, \mathbf{z}_a, Y^{(c)})$;

$\hat{Y}_v^{(f)} \leftarrow \mathcal{F}_{\mathcal{C}_v}(\mathbf{z}_v)$;

$\hat{Y}_a^{(f)} \leftarrow \mathcal{F}_{\mathcal{C}_a}(\mathbf{z}_a)$;

 /* FL: Frame Loss */

$\mathcal{L}_f \leftarrow \frac{1}{2}(\text{FL}(\hat{Y}_v^{(f)}, Y_v^{(f)}) + \text{FL}(\hat{Y}_a^{(f)}, Y_a^{(f)}))$;

 /* \oplus : concatenation */

$(\hat{Y}_v^{(b)(p)}, \hat{Y}_v^{(b)(c)}, \hat{Y}_v^{(b)(pc)}) \leftarrow \mathcal{F}_{\mathcal{B}_v}(\mathbf{z}_v \oplus \hat{Y}_v^{(f)})$;

$(\hat{Y}_a^{(b)(p)}, \hat{Y}_a^{(b)(c)}, \hat{Y}_a^{(b)(pc)}) \leftarrow \mathcal{F}_{\mathcal{B}_a}(\mathbf{z}_a \oplus \hat{Y}_a^{(f)})$;

$\hat{Y}^{(b)(p)} \leftarrow \mathcal{F}_{\Gamma_p}(\hat{Y}_v^{(b)(p)}, \hat{Y}_a^{(b)(p)}, \mathbf{z}_v, \mathbf{z}_a)$;

$\hat{Y}^{(b)(c)} \leftarrow \mathcal{F}_{\Gamma_c}(\hat{Y}_v^{(b)(c)}, \hat{Y}_a^{(b)(c)}, \mathbf{z}_v, \mathbf{z}_a)$;

$\hat{Y}^{(b)(pc)} \leftarrow \mathcal{F}_{\Gamma_{pc}}(\hat{Y}_v^{(b)(pc)}, \hat{Y}_a^{(b)(pc)}, \mathbf{z}_v, \mathbf{z}_a)$;

$\mathcal{L}_{bm} \leftarrow \frac{1}{2}(\text{MSE}(\hat{Y}_v^{(b)(p)}, Y_v^{(b)}) +$

$\text{MSE}(\hat{Y}_v^{(b)(c)}, Y_v^{(b)}) + \text{MSE}(\hat{Y}_v^{(b)(pc)}, Y_v^{(b)}) +$

$\text{MSE}(\hat{Y}_a^{(b)(p)}, Y_a^{(b)}) + \text{MSE}(\hat{Y}_a^{(b)(c)}, Y_a^{(b)}) +$

$\text{MSE}(\hat{Y}_a^{(b)(pc)}, Y_a^{(b)}))$;

$\mathcal{L}_b \leftarrow \text{MSE}(\hat{Y}^{(b)(p)}, Y^{(b)}) +$

$\text{MSE}(\hat{Y}^{(b)(c)}, Y^{(b)}) + \text{MSE}(\hat{Y}^{(b)(pc)}, Y^{(b)})$;

$\theta \leftarrow \text{Adam}(\mathcal{L}_b, \mathcal{L}_{bm}, \mathcal{L}_f, \mathcal{L}_c, \lambda, \theta)$;

end

return θ ;

4.4. Frame Classification Module

We further deploy frame-level classification modules on top of the visual and audio features. Let us denote the ground truth labels for visual and audio modality as $Y_v^{(f)}$ and $Y_a^{(f)}$. The visual classification module $\mathcal{F}_{\mathcal{C}_v}$ maps the latent visual features \mathbf{z}_v to labels $\hat{Y}_v^{(f)} \in \mathbb{R}^T$. Similarly, the audio classification module $\mathcal{F}_{\mathcal{C}_a}$ maps latent audio features

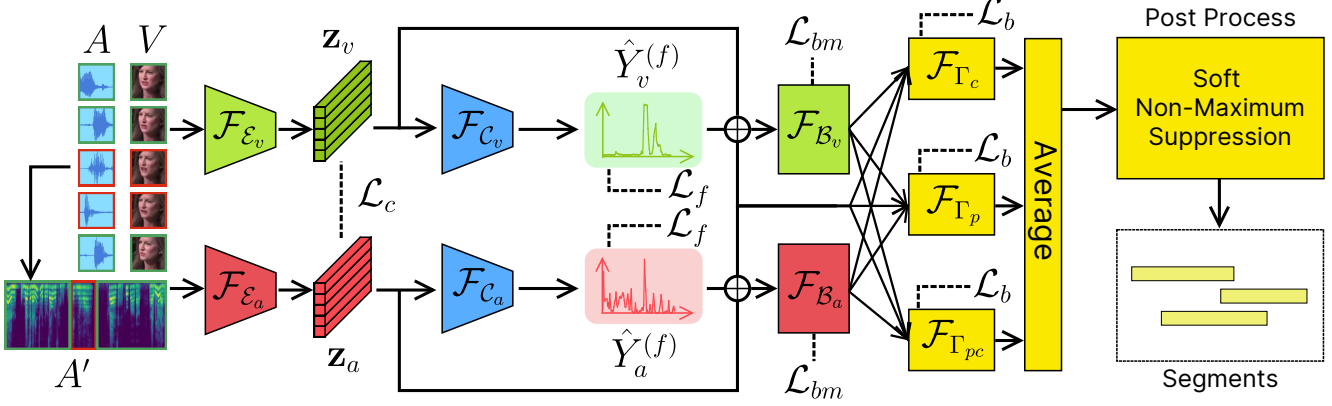


Figure 4. **Overview of the BA-TFD+ method.** BA-TFD+ mainly comprises of 1) Visual encoder (\mathcal{F}_{E_v}) that takes resized raw video frames as input, 2) Audio encoder (\mathcal{F}_{E_a}) that takes spectrogram extracted from raw audio as input, 3) Visual and audio based frame classification module (i.e. \mathcal{F}_{C_v} and \mathcal{F}_{C_a}), 4) Boundary localization module to facilitate forgery localization in both visual (\mathcal{F}_{B_v}) and audio (\mathcal{F}_{B_a}) modality, and finally 5) Multimodal fusion module that fuses multimodal latent features position-wise (p), channel-wise (c) and position-channel wise (pc). During inference, post-processing operation is applied to generate segments from the output of the fusion module. \oplus denotes concatenation.

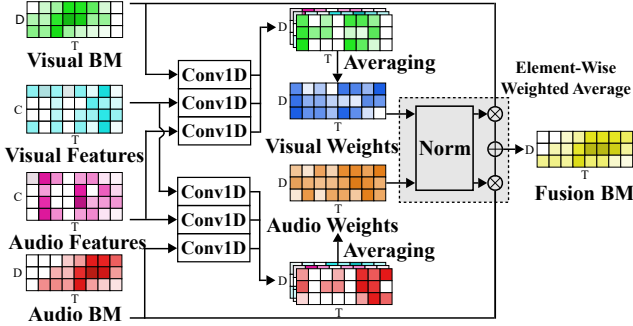


Figure 5. **Overview of the BA-TFD+ fusion module.** The gray block is used to normalize the visual and audio weights produced by the 1D convolutional layers, followed by element-wise weighted average. \oplus denotes element-wise addition, \otimes denotes element-wise multiplication and BM denotes boundary map.

\mathbf{z}_a to labels $\hat{Y}_a^{(f)} \in \mathbb{R}^T$.

4.5. Boundary Localization Module

This module facilitates the learning of deepfake localization. Motivated by BSN++ [86], we adopted the proposal relation block (PRB) as the framework for the boundary maps (representation of the boundary information of all densely distributed proposals). The ground truth boundary map $Y^{(b)} \in \mathbb{R}^{D \times T}$ is generated from Y , where $Y_{ij}^{(b)}$ is the confidence score for a segment which starts at the j -th frame and ends at the $(i+j)$ -th frame. The PRB module contains both a position-aware attention module (captures global dependencies) and a channel-aware attention module (captures inter-dependencies between different channels). In order to achieve localization in each modality, we deploy

two boundary modules, \mathcal{F}_{B_v} for visual and \mathcal{F}_{B_a} for audio modality.

The visual boundary module \mathcal{F}_{B_v} input consists of the concatenation of latent features \mathbf{z}_v and classification outputs $\hat{Y}_v^{(f)}$, i.e. $\mathbf{z}_v \oplus \hat{Y}_v^{(f)}$. \mathcal{F}_{B_v} predicts the position-aware boundary maps $\hat{Y}_v^{(b)(p)} \in \mathbb{R}^{D \times T}$ and the channel-aware boundary maps $\hat{Y}_v^{(b)(c)} \in \mathbb{R}^{D \times T}$ as output. These results are aggregated by a convolutional layer which outputs position-channel boundary maps denoted as $\hat{Y}_v^{(b)(pc)} \in \mathbb{R}^{D \times T}$. Similarly, the audio boundary module \mathcal{F}_{B_a} input consists of the concatenation of latent features \mathbf{z}_a and classification outputs $\hat{Y}_a^{(f)}$, i.e. $\mathbf{z}_a \oplus \hat{Y}_a^{(f)}$. \mathcal{F}_{B_a} first predicts the audio position-aware boundary maps $\hat{Y}_a^{(b)(p)}$ and channel-aware boundary maps $\hat{Y}_a^{(b)(c)}$. Then $\hat{Y}_a^{(b)(p)}$ and $\hat{Y}_a^{(b)(c)}$ are aggregated to $\hat{Y}_a^{(b)(pc)}$ using a convolutional layer.

4.6. Multimodal Fusion Module

The fusion module illustrated in Figure 5, uses boundary maps $\hat{Y}_v^{(b)(p)}$, $\hat{Y}_a^{(b)(p)}$, $\hat{Y}_v^{(b)(c)}$, $\hat{Y}_a^{(b)(c)}$, $\hat{Y}_v^{(b)(pc)}$, and $\hat{Y}_a^{(b)(pc)}$ and features \mathbf{z}_v and \mathbf{z}_a from the visual and audio modalities as input. Since the boundary module corresponding to each modality predicts three boundary maps, there are three fusion modules for position-aware \mathcal{F}_{Γ_p} , channel-aware \mathcal{F}_{Γ_c} and aggregated position-channel $\mathcal{F}_{\Gamma_{pc}}$ boundary maps.

For the visual modality, the visual boundary maps and features from the visual and audio modalities are used to calculate the visual weights $W_v \in \mathbb{R}^{D \times T}$. Similarly, for the audio modality, the audio boundary maps and features from both modalities are utilized to calculate the audio weights $W_a \in \mathbb{R}^{D \times T}$. The element-wise weighted average of

the fusion boundary maps predictions $\hat{Y}^{(b)(p)}$, $\hat{Y}^{(b)(c)}$ and $\hat{Y}^{(b)(pc)}$ is formed in the final step. Each boundary map $\alpha \in \{p, c, pc\}$ is calculated as follows,

$$\hat{Y}^{(b)(\alpha)} = \frac{W_v \hat{Y}_v^{(b)(\alpha)} + W_a \hat{Y}_a^{(b)(\alpha)}}{W_v + W_a},$$

where all operations are element-wise.

4.7. Loss Functions

The training process of BA-TFD+ is guided by contrastive (\mathcal{L}_c), frame classification (\mathcal{L}_f), boundary matching (\mathcal{L}_b) and multimodal boundary matching (\mathcal{L}_{bm}) loss functions.

4.7.1 Contrastive Loss

Contrastive loss has been proven to be helpful to eliminate the misalignment between different modalities [19,21]. Motivated by this, BA-TFD+ uses the latent visual and audio features \mathbf{z}_v and \mathbf{z}_a of real videos as positive pairs. On the other hand, latent features \mathbf{z}_v and \mathbf{z}_a with at least one modified modality are considered negative pairs (*i.e.* $Y^{(c)} = 0$). Thus, the contrastive loss minimizes the difference between the visual and audio modalities for positive pairs (*i.e.* $Y^{(c)} = 1$) and keeps that margin larger than δ for negative pairs. The contrastive loss is defined as follows,

$$\mathcal{L}_c = \frac{1}{C_f \sum \mathbb{T}} \sum_{i=1}^n Y_i^{(c)} d_i^2 + (1 - Y_i^{(c)}) \max(\delta - d_i, 0)^2$$

$$d_i = \|\mathbf{z}_{v_i} - \mathbf{z}_{a_i}\|_2,$$

where, n is the number of samples in the dataset, d_i is the ℓ_2 distance between visual and audio modality in the latent space, $Y_i^{(c)}$ is the label for contrastive learning and $\mathbb{T} = \{t_i\}_0^n$ where $\sum \mathbb{T}$ is the total number of frames in the dataset.

4.7.2 Frame Classification Loss

This is a standard frame level cross-entropy loss depicted as,

$$\mathcal{L}_f = -\frac{1}{2 \sum \mathbb{T}} \sum_{m \in \{a, v\}} \sum_{i=1}^n \sum_{j=1}^{t_i} H(\hat{Y}_{mij}^{(f)}, Y_{mij}^{(f)})$$

$$H(\hat{Y}^{(f)}, Y^{(f)}) = Y^{(f)} \log \hat{Y}^{(f)} + (1 - Y^{(f)}) \log (1 - \hat{Y}^{(f)})$$

$$Y_m^{(f)} = \eta_m Y^{(f)} + (1 - \eta_m) Y_\phi^{(f)},$$

where n is the number of samples in the dataset, t_i is the number of frames, m is the modality (*i.e.* audio a or visual

v), η_m specifies whether modality m is manipulated or not, $Y_\phi^{(f)} \in 0^T$ is the label for real videos, and $\mathbb{T} = \{t_i\}_0^n$ where $\sum \mathbb{T}$ is the total number of frames in the dataset. This loss enforces the visual and audio encoder to learn whether a visual frame or audio sample is real or fake.

4.7.3 Boundary Matching Loss

Following the standard protocol [57, 86], we generated the ground truth boundary maps as labels for efficient training. The fusion boundary matching loss is calculated as,

$$\mathcal{L}_b = \frac{1}{3D \sum \mathbb{T}} \sum_{\alpha \in \{p, c, pc\}} \sum_{i=1}^n \sum_{j=1}^D \sum_{k=1}^{t_i} (\hat{Y}_{ijk}^{(b)(\alpha)} - Y_{ijk}^{(b)})^2,$$

where α is one of the boundary map types from the boundary module, n is the number of samples in the dataset, D is the maximum proposal duration, t_i is the number of frames, and $\mathbb{T} = \{t_i\}_0^n$ where $\sum \mathbb{T}$ is the total number of frames in the dataset.

4.7.4 Multimodal Boundary Matching Loss

We utilized the label information for each modality to train the proposed multimodal framework and extended the concept of boundary matching loss (\mathcal{L}_b) to more modalities. The multimodal boundary matching loss is defined as follows,

$$\mathcal{L}_{bm} = \frac{1}{2D \sum \mathbb{T}} \sum_{m \in \{v, a\}} \sum_{\alpha \in \{p, c, pc\}} \sum_{i=1}^n \sum_{j=1}^D \sum_{k=1}^{t_i} (\hat{Y}_{mijk}^{(b)(\alpha)} - Y_{mijk}^{(b)})^2$$

$$Y_m^{(b)} = \eta_m Y^{(b)} + (1 - \eta_m) Y_\phi^{(b)},$$

where, m is the modality (visual v or audio a), η_m specifies whether modality m is modified, α is one of the boundary map types from the boundary module, $Y_\phi^{(b)} \in 0^{D \times T}$ is the ground truth boundary maps for real videos, and $\mathbb{T} = \{t_i\}_0^n$ where $\sum \mathbb{T}$ is the total number of frames in the dataset.

4.7.5 Overall Loss

The overall training objective of BA-TFD+ is defined as,

$$\mathcal{L} = \mathcal{L}_b + \lambda_{bm} \mathcal{L}_{bm} + \lambda_f \mathcal{L}_f + \lambda_c \mathcal{L}_c,$$

where, λ_{bm} , λ_f and λ_c are weights for different losses.

Table 3. **Temporal forgery localization results on the “fullset” of the LAV-DF dataset.** The visual-only version of BA-TFD+ uses the output from the visual boundary matching layer, illustrating the performance when using only the visual modality.

Method	AP@0.5	AP@0.75	AP@0.95	AR@100	AR@50	AR@20	AR@10
BMN [57]	10.56	01.66	00.00	48.49	44.39	37.13	31.55
BMN (E2E)	24.01	07.61	00.07	53.26	41.24	31.60	26.93
MDS [19]	12.78	01.62	00.00	37.88	36.71	34.39	32.15
AGT [67]	17.85	09.42	00.11	43.15	34.23	24.59	16.71
BSN++ [86]	56.41	32.57	00.21	74.93	71.11	64.98	59.29
AVFusion [3]	65.38	23.89	00.11	62.98	59.26	54.80	52.11
BA-TFD [12]	79.15	38.57	00.24	67.03	64.18	60.89	58.51
TadTR [62]	80.22	61.04	05.22	72.50	72.50	70.56	69.18
ActionFormer [99]	85.23	59.05	00.93	77.23	77.23	77.19	76.93
TriDet [82]	86.33	70.23	03.05	74.47	74.47	74.46	74.45
BA-TFD+ (ours)	96.30	84.96	04.44	81.62	80.48	79.40	78.75
BA-TFD+ (ours) (visual only)	64.78	54.85	02.53	64.00	59.33	55.94	54.38

Table 4. **Temporal forgery localization results on the “subset” of the LAV-DF dataset.** The visual-only version of BA-TFD+ uses the output from the visual boundary matching layer, illustrating the performance when using only the visual modality.

Method	AP@0.5	AP@0.75	AP@0.95	AR@100	AR@50	AR@20	AR@10
BMN [57]	28.10	05.47	00.01	55.49	54.44	52.14	47.72
BMN (E2E)	32.32	11.38	00.14	59.69	48.17	39.01	34.17
MDS [19]	23.43	03.48	00.00	58.53	56.68	53.16	49.67
AGT [67]	15.69	10.69	00.15	49.11	40.31	31.70	23.13
BSN++ [86]	65.26	37.70	00.22	78.89	76.32	71.00	65.38
AVFusion [3]	62.01	22.77	00.11	61.98	58.08	53.31	50.52
BA-TFD [12]	85.20	47.06	00.29	67.34	64.52	61.19	59.32
TadTR [62]	83.48	63.57	05.44	74.15	74.15	72.42	71.38
ActionFormer [99]	79.48	48.01	01.08	70.38	70.38	70.36	70.08
TriDet [82]	80.71	60.93	02.91	67.64	67.64	67.64	67.63
BA-TFD+ (ours)	96.82	86.47	03.90	81.74	80.59	79.60	79.15
BA-TFD+ (ours) (visual only)	96.47	82.02	03.79	80.65	79.00	77.46	76.90

4.8. Inference

During inference, the model generates three types of fusion boundary maps - position-aware boundary map $\hat{Y}^{(b)(p)}$, channel-aware boundary map $\hat{Y}^{(b)(c)}$ and aggregated position-channel boundary map $\hat{Y}^{(b)(pc)}$. Following previous work [86], we averaged the three boundary maps to produce the final boundary map $\hat{Y}^{(b)}$. This boundary map represents the confidence for all proposals in the video. Since this operation produces duplicated proposals, we post-process the proposals with Soft Non-Maximum Suppression (S-NMS) [7] similar to BSN++ [86].

5. Experiments

5.1. Dataset Partitioning

We splitted the LAV-DF dataset into 78,703 train, 31,501 validation and 26,100 test videos. The test partition is de-

noted as *full set*. For a fair comparison with existing visual-only methods [57, 86], we additionally prepared a subset of the full set denoted as *subset* where the audio-only manipulated videos are removed.

5.2. Implementation Details

The BA-TFD+ method is implemented in PyTorch [72] and the model is trained using 2 NVIDIA A100 80GB GPUs. We resized the input videos to 96×96 to reduce the computational cost of the MViT2-based visual backbone. The temporal dimension T is fixed to 512 for LAV-DF and 300 for ForgeryNet [37] and DFDC [26]. The latent features \mathbf{z}_v and \mathbf{z}_a have the same shape $C_f \times T$ where the feature size $C_f = 256$ and $T \in \{512, 300\}$. For the boundary matching modules $\mathcal{F}_{\mathcal{B}_v}$ and $\mathcal{F}_{\mathcal{B}_a}$, we set the maximum segment duration D to 40 for LAV-DF, 200 for ForgeryNet and 300 for DFDC. We followed the training protocol pro-

Table 5. **Temporal forgery localization results on the ForgeryNet dataset.** The visual-only version of BA-TFD+ uses the output from the visual boundary matching layer, illustrating the performance when using only the visual modality.

Method	Avg. AP	AP@0.5	AP@0.75	AP@0.95	AR@5	AR@2
Xception [18]	62.83	68.29	62.84	58.30	73.95	25.83
X3D-M+BSN [28, 59]	70.29	80.46	77.24	55.09	86.88	81.33
X3D-M+BMN [28, 57]	83.47	90.65	88.12	74.95	91.99	88.44
SlowFast+BSN [29, 59]	73.42	82.25	80.11	60.66	88.78	83.63
SlowFast+BMN [29, 57]	86.85	92.76	91.00	80.02	93.49	90.64
BA-TFD+ (ours) (visual only)	87.79	93.13	89.14	81.09	95.69	90.63

Table 6. **Deepfake detection results on the DFDC dataset.**

Method	AUC
Meso4 [1]	0.753
FWA [54]	0.727
Siamese [64]	0.844
MDS [19]	0.916
BA-TFD [12]	0.846
BA-TFD+ (ours)	0.937

posed in MViTv2 [55]. Throughout our experiments, we empirically set $\lambda_c = 0.1$, $\lambda_f = 2$, $\lambda_b = 1$, $\lambda_{bm} = 1$ and $\delta = 0.99$.

5.3. Evaluation Details

We benchmarked the LAV-DF dataset for deepfake detection and localization tasks. For deepfake detection we follow standard evaluation protocols [26, 76], and use Area Under the Curve (AUC) as evaluation metric for this binary classification task. We are the first to benchmark deepfake localization task and adopt Average Precision (AP) and Average Recall (AR) as the evaluation metrics. For AP, we set the IoU thresholds to 0.5, 0.75 and 0.95, following ActivityNet [10] evaluation protocol. For AR, since the number of fake segments is small, we set the number of proposals to 100, 50, 20 and 10 with the IoU thresholds [0.5:0.05:0.95]. When evaluating the proposed approach on ForgeryNet [37], we follow the protocol in that paper (i.e. AP@0.5, AP@0.75, AP@0.9, AR@5, and AR@2).

For evaluating BA-TFD+ on ForgeryNet, we used only the visual pipeline of the method to train the model (ForgeryNet is a visual-only deepfake dataset). Since only the visual modality is used in the model, only \mathcal{L}_b and \mathcal{L}_f are used for training. Similarly for evaluation on DFDC [26], we consider the whole fake video as one fake segment and train our model in the temporal localization manner. Then, we train a small MLP to map the boundary map to the final binary labels.

We also evaluated the performance of several state-of-the-art methods on LAV-DF, including BMN [57],

AGT [67], AVFusion [3], MDS [19], BSN++ [86], TadTR [62], ActionFormer [99], and TriDet [82]. Based on the original implementations, BMN, BSN++, TadTR, ActionFormer, and TriDet require extracted features, thus, we trained these models based on 2-stream I3D features [13]. For the methods that require S-NMS [7] during post-processing, we searched the optimal hyperparameters for S-NMS using the validation part of the concerned dataset. All reported results are based on the test partitions.

6. Results

6.1. Temporal Forgery Localization

6.1.1 LAV-DF Dataset

We evaluated the performance of BA-TFD+ on the LAV-DF dataset for temporal forgery localization, and compare it with other approaches. For the full set, from Table 3, our method achieves the best performance for AP@0.5 and AR@100. Unlike temporal action localization datasets, the segments in our dataset have a single label for the fake segments which leads to high AP scores. The multimodal MDS method is not specifically designed for temporal forgery localization tasks and can only predict fixed-length segments, lacking the ability to precisely identify boundaries. Therefore, the scores for MDS are relatively low. For BMN and BSN++, the AP scores are low because they are designed for fake proposal generation instead of forgery localization. TadTR, ActionFormer, and TriDet achieve relatively better performance as they are one-stage temporal action localization approaches that generate more precise segments. Additionally, we observe that BMN trained with an end-to-end visual encoder performs better than using pre-trained I3D features. With the multimodal complimentary information, our approach outperforms the aforementioned approaches.

We further evaluated all methods on the subset of the LAV-DF dataset. From Table 4, it is observed that the performance of the visual-only methods including BMN, AGT, BSN++ and TadTR is improved. The visual-only score of our method improves from 64.78 (AP@0.5) to 96.47 (AP@0.5), and the margin between the unimodal and multimodal versions is decreased significantly from

Table 7. **Impact of loss functions.** The contribution of different losses for temporal forgery localization on the full set of the LAV-DF dataset.

Loss Function	AP@0.5	AP@0.75	AP@0.95	AR@100	AR@50	AR@20	AR@10
\mathcal{L}_f	59.45	51.46	07.11	77.25	75.60	70.76	67.24
$\mathcal{L}_c, \mathcal{L}_f$	63.42	56.24	08.55	78.17	76.47	71.58	68.22
\mathcal{L}_b	71.31	34.30	00.12	66.92	63.67	57.99	54.72
$\mathcal{L}_{bm}, \mathcal{L}_b$	71.97	51.17	00.50	69.86	67.58	64.44	62.64
$\mathcal{L}_f, \mathcal{L}_{bm}, \mathcal{L}_b$	94.71	78.54	01.66	77.86	76.44	74.67	73.69
$\mathcal{L}_c, \mathcal{L}_f, \mathcal{L}_{bm}, \mathcal{L}_b$	96.30	84.96	04.44	81.62	80.48	79.40	78.75

Table 8. **Impact of pre-trained features.** Comparison of different pre-trained features for temporal forgery localization on the full set of the LAV-DF dataset.

Visual	Audio	Citation	AP@0.5	AP@0.75	AP@0.95	AR@100	AR@50	AR@20	AR@10
I3D	E2E	[13]	74.76	59.57	04.02	74.28	71.92	68.64	66.63
MARLIN	E2E	[11]	92.27	75.11	04.10	77.93	76.38	74.53	73.47
3DMM	E2E	[6]	01.84	00.11	00.00	34.00	31.54	20.94	11.81
E2E	TRILLsson3	[83]	95.16	82.67	05.65	81.21	79.80	78.22	77.49
E2E	Wav2Vec2	[2]	95.92	84.94	05.66	82.48	81.38	79.93	79.24
E2E	E2E	N/A	96.30	84.96	04.44	81.62	80.48	79.40	78.75

Table 9. **Impact of encoder architectures.** Comparison of different backbone architectures for temporal forgery localization on the full set of the LAV-DF dataset.

Visual	Audio	Boundary	AP@0.5	AP@0.75	AP@0.95	AR@100	AR@50	AR@20	AR@10
3D CNN	CNN	BMN	76.90	38.50	00.25	66.90	64.08	60.77	58.42
3D CNN	CNN	BSN++	92.44	71.34	01.15	75.86	74.43	72.39	71.21
MViTv2-Tiny	CNN	BMN	89.32	59.47	01.45	72.52	70.14	67.55	65.92
MViTv2-Small	CNN	BMN	89.31	59.97	01.78	72.74	70.35	67.56	65.87
MViTv2-Base	CNN	BMN	89.90	59.67	01.51	72.22	69.99	67.29	65.64
3D CNN	ViT-Tiny	BMN	78.08	35.18	00.41	67.38	64.38	60.92	58.66
3D CNN	ViT-Small	BMN	79.61	37.63	00.42	67.10	64.23	60.77	58.51
3D CNN	ViT-Base	BMN	80.86	36.55	00.34	67.24	64.27	60.86	58.46
MViTv2-Small	ViT-Base	BSN++	93.59	75.22	02.56	77.73	76.08	74.07	72.93
MViTv2-Base	ViT-Base	BSN++	96.30	84.96	04.44	81.62	80.48	79.40	78.75

31.52 (AP@0.5) to 0.35 (AP@0.5). Thus, our method demonstrates its superior performance for temporal forgery localization.

6.1.2 ForgeryNet Dataset

We evaluated the performance of the visual-only BA-TFD+ trained on the ForgeryNet dataset, and compare it with other approaches (using the results reported by [37]). As shown in Table 5, the performance of the visual-only BA-TFD+ exceeds the previous best model SlowFast [29]+BMN [57], showing that proposed method has advantage for temporal forgery localization.

6.2. Deepfake Detection

We also compare our method with previous deepfake detection methods on a subset of the DFDC dataset following the configuration of [19]. As shown in Table 6, the performance of our method is better than previous methods such as Meso4 [1], FWA [54], Siamese [64], and MDS [19]. In summary, our method performs well on the classification task.

6.3. Ablation Studies

6.3.1 Impact of Loss Functions

To examine the contributions of each loss of BA-TFD+, we train six models with different combinations of losses. To aggregate the frame-level predictions for the models without boundary module, we follow the algorithm proposed in

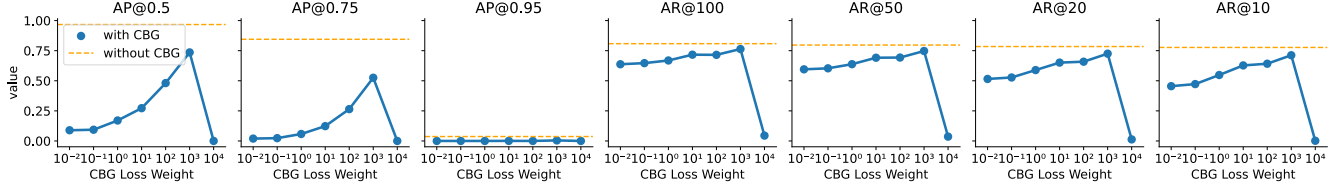


Figure 6. **Impact of CBG in the boundary matching module.** The figure shows comparison of models containing CBG module and a model without CBG module.

previous work [101]. From table 7, it is evident that all of the integrated losses have positive influence on the performance. By observing the difference between the scores, the boundary matching loss \mathcal{L}_b and the frame classification loss \mathcal{L}_c contribute significantly to the performance. With the frame-level labels supervising the model, the encoders are trained to have a better capacity to extract the features relevant to deepfake artifacts. Whereas the boundary module mechanism have localization ability to detect the fake segments more precisely.

6.3.2 Impact of Pre-Trained Features

In the literature [62, 99], pre-trained visual features, such as I3D [13], are commonly used for temporal action localization. Since the I3D features are pre-trained on the Kinetics dataset [45], they encode the representation of the universal scene of the video. However, temporal forgery localization requires the model to have a specialized understanding of facial information. Therefore, the pre-trained features obtained from universal visual dataset are not likely to be suitable for our task. Our quantitative results support this, e.g. the comparison between the two BMN models in Table 3 where one uses I3D features and the other uses end-to-end training.

To examine the impact of pre-trained features on BA-TFD+, we trained models using different pre-trained features, including visual (I3D, MARLIN ViT-S [11] and 3DMM [6]) and audio features (TRILLsson [83] and Wav2Vec2 [2]). The results are shown in Table 8. From the results, we can observe the following patterns: 1) The model trained fully end-to-end reaches the best performance and 2) Compared with visual features, audio features have better task specific performance.

6.3.3 Impact of Encoder Architectures

To find the best modality-specific architecture for BA-TFD+, we trained several architecture combinations for the visual encoder, audio encoder, and boundary module. The results are presented in Table 9. Compared to the previous model BA-TFD [12] as baseline (3D-CNN + CNN + BMN [57]), we used the attention-based architectures including MViTv2 [55] and ViT [27] families for encoders

and attention-based BSN++ modules [86] for predicting boundaries.

We used the variations of MViTv2 from the original paper (*i.e.* MViTv2-Tiny, MViTv2-Small and MViTv2-Base) as the visual encoders. We can conclude that the MViTv2 architecture plays an important role while comparing with the baseline, but the benefit of different scales of the MViTv2 architecture is not significant. As for the audio encoder, we followed the architecture definitions for ViT (*i.e.* ViT-Tiny, ViT-Small and ViT-Base) for comparison. We can conclude that the audio encoder benefits from different scales of the ViT architecture. We also compared the BSN++-based boundary module with BMN-based architecture. The contribution from the BSN++ is the most significant compared with MViTv2 for the visual encoder and ViT for the audio encoder. Owing to the attention mechanism, the framework utilizes the global and local context to analyze the artifacts. The combination of MViTv2-Base, ViT-Base and BSN++ produces the best performance compared to all other combinations of modules.

6.3.4 Impact of CBG in the Boundary Matching Module

We adopted the method from BSN++ [86] to improve the performance for temporal forgery localization. This method includes two modules, complementary boundary generator (CBG) and proposal relation block (PRB). The CBG module predicts the confidence that a timestamp is starting or ending point of segments. The PRB module, based on BMN [57], predicts the boundary map which contains the confidences of dense segment proposals. For inference, the results from both modules are multiplied as the final output. In this ablation study, we aim to discuss the impact of the CBG module.

We trained several models containing CBG modules with different loss weights, from 10^{-2} to 10^4 , and also a model without CBG module. As shown in Figure 6, the best CBG loss weight is 10^3 . However, compared with the non-CBG model, the best model with CBG can only compete on AR and has a huge gap on AP metrics. Based on this observation, we drop the CBG module in the boundary module and only use PRB.

7. Conclusion

In this paper, we introduce and investigate content-driven multimodal deepfake generation, detection, and localization. We introduce a new dataset where both the audio and visual modalities are modified at strategic locations. Additionally, we propose a new method for temporal forgery localization. Through extensive experiments, we demonstrate that our method outperforms existing state-of-the-art techniques.

The proposed dataset, LAV-DF, may raise ethical concerns due to its potential negative social impact. Given that the dataset contains facial videos of celebrities, there could be a risk of its misuse for unethical purposes. Moreover, the dataset generation pipeline itself can be used to generate fake videos. To confront the potential negative impact of our work, we have taken several measures. Most importantly, we have prepared an end-user license agreement as a preventive measure. Similarly, users need to agree on terms and conditions to use the proposed temporal forgery localization method BA-TFD+.

This work has some limitations: 1) The audio reenactment method employed for dataset creation does not consistently generate the desired reference style, 2) The resolution of the dataset is limited by the source videos, and 3) The high classification scores obtained indicate the need for further improvement in the visual reenactment method.

Major improvement in the future will be extending the generation pipeline to include word tokens insertion, substitution and deletion and converting statements into questions.

References

- [1] Darius Afchar, Vincent Nozick, Junichi Yamagishi, and Isao Echizen. MesoNet: a Compact Facial Video Forgery Detection Network. In *2018 IEEE International Workshop on Information Forensics and Security (WIFS)*, pages 1–7, Dec. 2018. ISSN: 2157-4774.
- [2] Alexei Baevski, Yuhao Zhou, Abdelrahman Mohamed, and Michael Auli. wav2vec 2.0: A Framework for Self-Supervised Learning of Speech Representations. In *Advances in Neural Information Processing Systems*, volume 33, pages 12449–12460. Curran Associates, Inc., 2020.
- [3] Anurag Bagchi, Jazib Mahmood, Dolton Fernandes, and Ravi Sarvadevabhatla. Hear Me out: Fusional Approaches for Audio Augmented Temporal Action Localization. In *Proceedings of the 17th International Joint Conference on Computer Vision, Imaging and Computer Graphics Theory and Applications*, pages 144–154. SCITEPRESS - Science and Technology Publications, 2022.
- [4] Belhassen Bayar and Matthew C. Stamm. A Deep Learning Approach to Universal Image Manipulation Detection Using a New Convolutional Layer. In *Proceedings of the 4th ACM Workshop on Information Hiding and Multimedia Security, IH&MMSec '16*, pages 5–10, New York, NY, USA, June 2016. Association for Computing Machinery.
- [5] Steven Bird, Ewan Klein, and Edward Loper. *Natural Language Processing with Python: Analyzing Text with the Natural Language Toolkit*. O'Reilly Media, Inc., June 2009. Google-Books-ID: KG1bfiiP1i4C.
- [6] Volker Blanz and Thomas Vetter. A morphable model for the synthesis of 3D faces. In *Proceedings of the 26th annual conference on Computer graphics and interactive techniques - SIGGRAPH '99*, pages 187–194, Not Known, 1999. ACM Press.
- [7] Navaneeth Bodla, Bharat Singh, Rama Chellappa, and Larry S. Davis. Soft-NMS – Improving Object Detection With One Line of Code. In *Proceedings of the IEEE International Conference on Computer Vision*, pages 5561–5569, 2017.
- [8] John Brandon. There Are Now 15,000 Deepfake Videos on Social Media. Yes, You Should Worry. *Forbes*, Oct. 2019.
- [9] Shyamal Buch, Victor Escorcia, Bernard Ghanem, Li Fei-Fei, and Juan Carlos Niebles. End-to-end, single-stream temporal action detection in untrimmed videos. *Proceedings of the British Machine Vision Conference 2017*, May 2019. Publisher: British Machine Vision Association.
- [10] Fabian Caba Heilbron, Victor Escorcia, Bernard Ghanem, and Juan Carlos Niebles. ActivityNet: A Large-Scale Video Benchmark for Human Activity Understanding. In *Proceedings of the IEEE Conference on Computer Vision and Pattern Recognition*, pages 961–970, 2015.
- [11] Zhixi Cai, Shreya Ghosh, Kalin Stefanov, Abhinav Dhall, Jianfei Cai, Hamid Rezatofighi, Reza Haffari, and Munawar Hayat. MARLIN: Masked Autoencoder for Facial Video Representation Learning. In *Proceedings of the IEEE/CVF Conference on Computer Vision and Pattern Recognition*, pages 1493–1504, 2023.
- [12] Zhixi Cai, Kalin Stefanov, Abhinav Dhall, and Munawar Hayat. Do You Really Mean That? Content Driven Audio-Visual Deepfake Dataset and Multimodal Method for Temporal Forgery Localization. In *2022 International Conference on Digital Image Computing: Techniques and Applications (DICTA)*, pages 1–10, Nov. 2022.

- [13] Joao Carreira and Andrew Zisserman. Quo Vadis, Action Recognition? A New Model and the Kinetics Dataset. In *Proceedings of the IEEE Conference on Computer Vision and Pattern Recognition*, pages 6299–6308, 2017.
- [14] Edresson Casanova, Christopher Shulby, Eren Gölge, Nicolas Michael Müller, Frederico Santos De Oliveira, Arnaldo Candido Jr., Anderson Da Silva Soares, Sandra Maria Aluisio, and Moacir Antonelli Ponti. SC-GlowTTS: An Efficient Zero-Shot Multi-Speaker Text-To-Speech Model. In *Interspeech 2021*, pages 3645–3649. ISCA, Aug. 2021.
- [15] Beijing Chen, Tianmu Li, and Weiping Ding. Detecting deepfake videos based on spatiotemporal attention and convolutional LSTM. *Information Sciences*, 601:58–70, July 2022.
- [16] Lele Chen, Guofeng Cui, Celong Liu, Zhong Li, Ziyi Kou, Yi Xu, and Chenliang Xu. Talking-Head Generation with Rhythmic Head Motion. In Andrea Vedaldi, Horst Bischof, Thomas Brox, and Jan-Michael Frahm, editors, *Computer Vision – ECCV 2020*, Lecture Notes in Computer Science, pages 35–51, Cham, 2020. Springer International Publishing.
- [17] Lele Chen, Ross K. Maddox, Zhiyao Duan, and Chenliang Xu. Hierarchical Cross-Modal Talking Face Generation With Dynamic Pixel-Wise Loss. In *Proceedings of the IEEE/CVF Conference on Computer Vision and Pattern Recognition*, pages 7832–7841, 2019.
- [18] Francois Chollet. Xception: Deep Learning With Depthwise Separable Convolutions. In *Proceedings of the IEEE Conference on Computer Vision and Pattern Recognition*, pages 1251–1258, 2017.
- [19] Komal Chugh, Parul Gupta, Abhinav Dhall, and Ramanathan Subramanian. Not made for each other: Audio-Visual Dissonance-based Deepfake Detection and Localization. In *Proceedings of the 28th ACM International Conference on Multimedia*, MM ’20, pages 439–447, New York, NY, USA, Oct. 2020. Association for Computing Machinery.
- [20] Joon Son Chung, Arsha Nagrani, and Andrew Zisserman. VoxCeleb2: Deep Speaker Recognition. In *Interspeech 2018*, pages 1086–1090. ISCA, Sept. 2018.
- [21] Joon Son Chung and Andrew Zisserman. Out of Time: Automated Lip Sync in the Wild. In Chu-Song Chen, Jiwen Lu, and Kai-Kuang Ma, editors, *Computer Vision – ACCV 2016 Workshops*, Lecture Notes in Computer Science, pages 251–263, Cham, 2017. Springer International Publishing.
- [22] Davide Alessandro Coccomini, Nicola Messina, Claudio Gennaro, and Fabrizio Falchi. Combining EfficientNet and Vision Transformers for Video Deepfake Detection. In Stan Sclaroff, Cosimo Distanto, Marco Leo, Giovanni M. Farinella, and Federico Tombari, editors, *Image Analysis and Processing – ICIAP 2022*, Lecture Notes in Computer Science, pages 219–229, Cham, 2022. Springer International Publishing.
- [23] Davide Cozzolino, Giovanni Poggi, and Luisa Verdoliva. Recasting Residual-based Local Descriptors as Convolutional Neural Networks: an Application to Image Forgery Detection. In *Proceedings of the 5th ACM Workshop on Information Hiding and Multimedia Security*, IH&MMSec ’17, pages 159–164, New York, NY, USA, June 2017. Association for Computing Machinery.
- [24] Dima Damen, Hazel Doughty, Giovanni Maria Farinella, Antonino Furnari, Evangelos Kazakos, Jian Ma, Davide Moltisanti, Jonathan Munro, Toby Perrett, Will Price, and Michael Wray. Rescaling Egocentric Vision: Collection, Pipeline and Challenges for EPIC-KITCHENS-100. *International Journal of Computer Vision*, 130(1):33–55, Jan. 2022.
- [25] Oscar de Lima, Sean Franklin, Shreshtha Basu, Blake Karwoski, and Annet George. Deepfake Detection using Spatiotemporal Convolutional Networks, June 2020. arXiv:2006.14749 [cs, eess].
- [26] Brian Dolhansky, Joanna Bitton, Ben Pfau, Jikuo Lu, Russ Howes, Menglin Wang, and Cristian Canton Ferrer. The DeepFake Detection Challenge (DFDC) Dataset, Oct. 2020. arXiv: 2006.07397 [cs].
- [27] Alexey Dosovitskiy, Lucas Beyer, Alexander Kolesnikov, Dirk Weissenborn, Xiaohua Zhai, Thomas Unterthiner, Mostafa Dehghani, Matthias Minderer, Georg Heigold, Sylvain Gelly, Jakob Uszkoreit, and Neil Houlsby. An Image is Worth 16x16 Words: Transformers for Image Recognition at Scale. In *International Conference on Learning Representations*, 2021.
- [28] Christoph Feichtenhofer. X3D: Expanding Architectures for Efficient Video Recognition. In *Proceedings of the IEEE/CVF Conference on Computer Vision and Pattern Recognition*, pages 203–213, 2020.
- [29] Christoph Feichtenhofer, Haoqi Fan, Jitendra Malik, and Kaiming He. SlowFast Networks for Video Recognition. In *Proceedings of the IEEE/CVF International Conference on Computer Vision*, pages 6202–6211, 2019.
- [30] Christiane Fellbaum. *WordNet: An Electronic Lexical Database*. MIT Press, 1998. Google-Books-ID: Rehu800zMIMC.

- [31] Jiyang Gao, Kan Chen, and Ram Nevatia. CTAP: Complementary Temporal Action Proposal Generation. In *Proceedings of the European Conference on Computer Vision (ECCV)*, pages 68–83, 2018.
- [32] Jiyang Gao, Zhenheng Yang, Kan Chen, Chen Sun, and Ram Nevatia. TURN TAP: Temporal Unit Regression Network for Temporal Action Proposals. In *Proceedings of the IEEE International Conference on Computer Vision*, pages 3628–3636, 2017.
- [33] Ian Goodfellow, Jean Pouget-Abadie, Mehdi Mirza, Bing Xu, David Warde-Farley, Sherjil Ozair, Aaron Courville, and Yoshua Bengio. Generative adversarial networks. *Communications of the ACM*, 63(11):139–144, Oct. 2020.
- [34] Zhihao Gu, Yang Chen, Taiping Yao, Shouhong Ding, Jilin Li, Feiyue Huang, and Lizhuang Ma. Spatiotemporal Inconsistency Learning for DeepFake Video Detection. In *Proceedings of the 29th ACM International Conference on Multimedia*, pages 3473–3481. Association for Computing Machinery, New York, NY, USA, Oct. 2021.
- [35] Luca Guarnera, Oliver Giudice, and Sebastiano Battiato. DeepFake Detection by Analyzing Convolutional Traces. In *Proceedings of the IEEE/CVF Conference on Computer Vision and Pattern Recognition Workshops*, pages 666–667, 2020.
- [36] Yudong Guo, Keyu Chen, Sen Liang, Yong-Jin Liu, Hujun Bao, and Juyong Zhang. AD-NeRF: Audio Driven Neural Radiance Fields for Talking Head Synthesis. In *Proceedings of the IEEE/CVF International Conference on Computer Vision*, pages 5784–5794, 2021.
- [37] Yanan He, Bei Gan, Siyu Chen, Yichun Zhou, Guojun Yin, Luchuan Song, Lu Sheng, Jing Shao, and Ziwei Liu. ForgeryNet: A Versatile Benchmark for Comprehensive Forgery Analysis. In *Proceedings of the IEEE/CVF Conference on Computer Vision and Pattern Recognition*, pages 4360–4369, 2021.
- [38] Young-Jin Heo, Woon-Ha Yeo, and Byung-Gyu Kim. DeepFake detection algorithm based on improved vision transformer. *Applied Intelligence*, 53(7):7512–7527, Apr. 2023.
- [39] Haroon Idrees, Amir R. Zamir, Yu-Gang Jiang, Alex Gorban, Ivan Laptev, Rahul Sukthankar, and Mubarak Shah. The THUMOS Challenge on Action Recognition for Videos ”in the Wild”. *Computer Vision and Image Understanding*, 155:1–23, Feb. 2017. arXiv: 1604.06182.
- [40] Hafsa Ilyas, Ali Javed, and Khalid Mahmood Malik. AVFakeNet: A unified end-to-end Dense Swin Transformer deep learning model for audio–visual deepfakes detection. *Applied Soft Computing*, 136:110124, Mar. 2023.
- [41] Amir Jamaludin, Joon Son Chung, and Andrew Zisserman. You Said That?: Synthesising Talking Faces from Audio. *International Journal of Computer Vision*, 127(11):1767–1779, Dec. 2019.
- [42] Ye Jia, Yu Zhang, Ron J. Weiss, Quan Wang, Jonathan Shen, Fei Ren, Zhifeng Chen, Patrick Nguyen, Ruoming Pang, Ignacio Lopez Moreno, and Yonghui Wu. Transfer learning from speaker verification to multispeaker text-to-speech synthesis. In *Proceedings of the 32nd International Conference on Neural Information Processing Systems, NIPS’18*, pages 4485–4495, Red Hook, NY, USA, Dec. 2018. Curran Associates Inc.
- [43] Liming Jiang, Ren Li, Wayne Wu, Chen Qian, and Chen Change Loy. DeeperForensics-1.0: A Large-Scale Dataset for Real-World Face Forgery Detection. In *Proceedings of the IEEE/CVF Conference on Computer Vision and Pattern Recognition*, pages 2889–2898, 2020.
- [44] Prajwal K R, Rudrabha Mukhopadhyay, Jerin Philip, Abhishek Jha, Vinay Namboodiri, and C V Jawahar. Towards Automatic Face-to-Face Translation. In *Proceedings of the 27th ACM International Conference on Multimedia, MM ’19*, pages 1428–1436, New York, NY, USA, Oct. 2019. Association for Computing Machinery.
- [45] Will Kay, Joao Carreira, Karen Simonyan, Brian Zhang, Chloe Hillier, Sudheendra Vijayanarasimhan, Fabio Viola, Tim Green, Trevor Back, Paul Natsev, Mustafa Suleyman, and Andrew Zisserman. The Kinetics Human Action Video Dataset, May 2017. arXiv:1705.06950 [cs].
- [46] Hasam Khalid, Minha Kim, Shahroz Tariq, and Simon S. Woo. Evaluation of an Audio-Video Multimodal Deepfake Dataset using Unimodal and Multimodal Detectors. *Proceedings of the 1st Workshop on Synthetic Multimedia - Audiovisual Deepfake Generation and Detection*, pages 7–15, Oct. 2021. arXiv: 2109.02993.
- [47] Hasam Khalid, Shahroz Tariq, and Simon S. Woo. FakeAVCeleb: A Novel Audio-Video Multimodal Deepfake Dataset, Aug. 2021. arXiv: 2108.05080 [cs].
- [48] Davis E. King. Dlib-ml: A Machine Learning Toolkit. *The Journal of Machine Learning Research*, 10:1755–1758, Dec. 2009.
- [49] Pavel Korshunov and Sebastien Marcel. DeepFakes: a New Threat to Face Recognition? Assessment and Detection, Dec. 2018. arXiv:1812.08685 [cs].

- [50] Iryna Korshunova, Wenzhe Shi, Joni Dambre, and Lucas Theis. Fast Face-Swap Using Convolutional Neural Networks. In *Proceedings of the IEEE International Conference on Computer Vision*, pages 3677–3685, 2017.
- [51] Patrick Kwon, Jaeseong You, Gyuhyeon Nam, Sungwoo Park, and Gyeongsu Chae. KoDF: A Large-Scale Korean DeepFake Detection Dataset. In *Proceedings of the IEEE/CVF International Conference on Computer Vision*, pages 10744–10753, 2021.
- [52] John K. Lewis, Imad Eddine Toubal, Helen Chen, Vishal Sandesera, Michael Lomnitz, Zigfried Hampel-Arias, Calyam Prasad, and Kannappan Palaniappan. Deepfake Video Detection Based on Spatial, Spectral, and Temporal Inconsistencies Using Multimodal Deep Learning. In *2020 IEEE Applied Imagery Pattern Recognition Workshop (AIPR)*, pages 1–9, Mar. 2020. ISSN: 2332-5615.
- [53] Lingzhi Li, Jianmin Bao, Ting Zhang, Hao Yang, Dong Chen, Fang Wen, and Baining Guo. Face X-Ray for More General Face Forgery Detection. In *Proceedings of the IEEE/CVF Conference on Computer Vision and Pattern Recognition*, pages 5001–5010, 2020.
- [54] Yuezun Li and Siwei Lyu. Exposing DeepFake Videos By Detecting Face Warping Artifacts. In *IEEE Conference on Computer Vision and Pattern Recognition Workshops (CVPRW)*, page 7, 2019.
- [55] Yanghao Li, Chao-Yuan Wu, Haoqi Fan, Kartikeya Mangalam, Bo Xiong, Jitendra Malik, and Christoph Feichtenhofer. MViTv2: Improved Multiscale Vision Transformers for Classification and Detection. In *Proceedings of the IEEE/CVF Conference on Computer Vision and Pattern Recognition*, pages 4804–4814, 2022.
- [56] Yuezun Li, Xin Yang, Pu Sun, Honggang Qi, and Siwei Lyu. Celeb-DF: A Large-Scale Challenging Dataset for DeepFake Forensics. In *Proceedings of the IEEE/CVF Conference on Computer Vision and Pattern Recognition*, pages 3207–3216, 2020.
- [57] Tianwei Lin, Xiao Liu, Xin Li, Errui Ding, and Shilei Wen. BMN: Boundary-Matching Network for Temporal Action Proposal Generation. In *Proceedings of the IEEE/CVF International Conference on Computer Vision*, pages 3889–3898, 2019.
- [58] Tianwei Lin, Xu Zhao, and Zheng Shou. Single Shot Temporal Action Detection. In *Proceedings of the 25th ACM international conference on Multimedia*, MM '17, pages 988–996, New York, NY, USA, Oct. 2017. Association for Computing Machinery.
- [59] Tianwei Lin, Xu Zhao, Haisheng Su, Chongjing Wang, and Ming Yang. BSN: Boundary Sensitive Network for Temporal Action Proposal Generation. In *Proceedings of the European Conference on Computer Vision (ECCV)*, pages 3–19, 2018.
- [60] Xiaolong Liu, Song Bai, and Xiang Bai. An Empirical Study of End-to-End Temporal Action Detection. In *Proceedings of the IEEE/CVF Conference on Computer Vision and Pattern Recognition*, pages 20010–20019, 2022.
- [61] Xiaolong Liu, Yao Hu, Song Bai, Fei Ding, Xiang Bai, and Philip H. S. Torr. Multi-Shot Temporal Event Localization: A Benchmark. In *Proceedings of the IEEE/CVF Conference on Computer Vision and Pattern Recognition*, pages 12596–12606, 2021.
- [62] Xiaolong Liu, Qimeng Wang, Yao Hu, Xu Tang, Shiwei Zhang, Song Bai, and Xiang Bai. End-to-End Temporal Action Detection With Transformer. *IEEE Transactions on Image Processing*, 31:5427–5441, 2022. Conference Name: IEEE Transactions on Image Processing.
- [63] Yi Liu, Limin Wang, Yali Wang, Xiao Ma, and Yu Qiao. FineAction: A Fine-Grained Video Dataset for Temporal Action Localization. *IEEE Transactions on Image Processing*, 31:6937–6950, 2022. Conference Name: IEEE Transactions on Image Processing.
- [64] Trisha Mittal, Uttaran Bhattacharya, Rohan Chandra, Aniket Bera, and Dinesh Manocha. Emotions Don't Lie: An Audio-Visual Deepfake Detection Method using Affective Cues. In *Proceedings of the 28th ACM International Conference on Multimedia*, MM '20, pages 2823–2832, New York, NY, USA, Oct. 2020. Association for Computing Machinery.
- [65] Daniel Mas Montserrat, Hanxiang Hao, Sri K. Yarlagadda, Sriram Baireddy, Ruiting Shao, Janos Horvath, Emily Bartusiak, Justin Yang, David Guera, Fengqing Zhu, and Edward J. Delp. Deepfakes Detection With Automatic Face Weighting. In *Proceedings of the IEEE/CVF Conference on Computer Vision and Pattern Recognition Workshops*, pages 668–669, 2020.
- [66] Kartik Narayan, Harsh Agarwal, Kartik Thakral, Surbhi Mittal, Mayank Vatsa, and Richa Singh. DF-Platter: Multi-Face Heterogeneous Deepfake Dataset. In *Proceedings of the IEEE/CVF Conference on Computer Vision and Pattern Recognition*, pages 9739–9748, 2023.
- [67] Megha Nawhal and Greg Mori. Activity Graph Transformer for Temporal Action Localization. *arXiv:2101.08540 [cs]*, Jan. 2021. arXiv: 2101.08540.

- [68] Paarth Neekhara, Shehzeen Hussain, Shlomo Dubnov, Farinaz Koushanfar, and Julian McAuley. Expressive Neural Voice Cloning. In *Proceedings of The 13th Asian Conference on Machine Learning*, pages 252–267. PMLR, Nov. 2021. ISSN: 2640-3498.
- [69] Dufou Nick and Jigsaw Andrew. Contributing Data to Deepfake Detection Research, Sept. 2019.
- [70] Yuval Nirkin, Yosi Keller, and Tal Hassner. FS-GAN: Subject Agnostic Face Swapping and Reenactment. In *Proceedings of the IEEE/CVF International Conference on Computer Vision*, pages 7184–7193, 2019.
- [71] Aaron van den Oord, Sander Dieleman, Heiga Zen, Karen Simonyan, Oriol Vinyals, Alex Graves, Nal Kalchbrenner, Andrew Senior, and Koray Kavukcuoglu. WaveNet: A Generative Model for Raw Audio, Sept. 2016. arXiv:1609.03499 [cs].
- [72] Adam Paszke, Sam Gross, Francisco Massa, Adam Lerer, James Bradbury, Gregory Chanan, Trevor Killeen, Zeming Lin, Natalia Gimelshein, Luca Antiga, Alban Desmaison, Andreas Kopf, Edward Yang, Zachary DeVito, Martin Raison, Alykhan Tejani, Sasank Chilamkurthy, Benoit Steiner, Lu Fang, Junjie Bai, and Soumith Chintala. PyTorch: An Imperative Style, High-Performance Deep Learning Library. In *Advances in Neural Information Processing Systems*, volume 32. Curran Associates, Inc., 2019.
- [73] K R Prajwal, Rudrabha Mukhopadhyay, Vinay P. Namboodiri, and C.V. Jawahar. A Lip Sync Expert Is All You Need for Speech to Lip Generation In the Wild. In *Proceedings of the 28th ACM International Conference on Multimedia*, MM '20, pages 484–492, New York, NY, USA, Oct. 2020. Association for Computing Machinery.
- [74] Yuyang Qian, Guojun Yin, Lu Sheng, Zixuan Chen, and Jing Shao. Thinking in Frequency: Face Forgery Detection by Mining Frequency-Aware Clues. In Andrea Vedaldi, Horst Bischof, Thomas Brox, and Jan-Michael Frahm, editors, *Computer Vision – ECCV 2020*, Lecture Notes in Computer Science, pages 86–103, Cham, 2020. Springer International Publishing.
- [75] Muhammad Anas Raza and Khalid Mahmood Malik. Multimodaltrace: Deepfake Detection Using Audio-visual Representation Learning. In *Proceedings of the IEEE/CVF Conference on Computer Vision and Pattern Recognition*, pages 993–1000, 2023.
- [76] Andreas Rossler, Davide Cozzolino, Luisa Verdoliva, Christian Riess, Justus Thies, and Matthias Niessner. FaceForensics++: Learning to Detect Manipulated Facial Images. In *Proceedings of the IEEE/CVF International Conference on Computer Vision*, pages 1–11, 2019.
- [77] David E. Rumelhart, Geoffrey E. Hinton, and Ronald J. Williams. Learning Internal Representations by Error Propagation. Technical report, CALIFORNIA UNIV SAN DIEGO LA JOLLA INST FOR COGNITIVE SCIENCE, Sept. 1985. Section: Technical Reports.
- [78] Ian Sample. What are deepfakes – and how can you spot them? *The Guardian*, Jan. 2020.
- [79] Conrad Sanderson, editor. *The VidTIMIT Database*. IDIAP, 2002.
- [80] Oscar Schwartz. You thought fake news was bad? Deep fakes are where truth goes to die. *The Guardian*, Nov. 2018.
- [81] Jonathan Shen, Ruoming Pang, Ron J. Weiss, Mike Schuster, Navdeep Jaitly, Zongheng Yang, Zhifeng Chen, Yu Zhang, Yuxuan Wang, Rj Skerrv-Ryan, Rif A. Saurous, Yannis Agiomvrgiannakis, and Yonghui Wu. Natural TTS Synthesis by Conditioning Wavenet on MEL Spectrogram Predictions. In *2018 IEEE International Conference on Acoustics, Speech and Signal Processing (ICASSP)*, pages 4779–4783, Apr. 2018. ISSN: 2379-190X.
- [82] Dingfeng Shi, Yujie Zhong, Qiong Cao, Lin Ma, Jia Li, and Dacheng Tao. TriDet: Temporal Action Detection With Relative Boundary Modeling. In *Proceedings of the IEEE/CVF Conference on Computer Vision and Pattern Recognition*, pages 18857–18866, 2023.
- [83] Joel Shor and Subhashini Venugopalan. TRILLsson: Distilled Universal Paralinguistic Speech Representations. In *Interspeech 2022*, pages 356–360, Sept. 2022. arXiv:2203.00236 [cs, eess].
- [84] Zheng Shou, Jonathan Chan, Alireza Zareian, Kazuyuki Miyazawa, and Shih-Fu Chang. CDC: Convolutional-De-Convolutional Networks for Precise Temporal Action Localization in Untrimmed Videos. In *Proceedings of the IEEE Conference on Computer Vision and Pattern Recognition*, pages 5734–5743, 2017.
- [85] Zheng Shou, Dongang Wang, and Shih-Fu Chang. Temporal Action Localization in Untrimmed Videos via Multi-Stage CNNs. In *Proceedings of the IEEE Conference on Computer Vision and Pattern Recognition*, pages 1049–1058, 2016.
- [86] Haisheng Su, Weihao Gan, Wei Wu, Yu Qiao, and Junjie Yan. BSN++: Complementary Boundary Regressor with Scale-Balanced Relation Modeling for Temporal Action Proposal Generation. *Proceedings*

of the *AAAI Conference on Artificial Intelligence*, 35(3):2602–2610, May 2021. Number: 3.

- [87] Justus Thies, Mohamed Elgharib, Ayush Tewari, Christian Theobalt, and Matthias Nießner. Neural Voice Puppetry: Audio-Driven Facial Reenactment. In Andrea Vedaldi, Horst Bischof, Thomas Brox, and Jan-Michael Frahm, editors, *ECCV 2020*, Lecture Notes in Computer Science, pages 716–731, Cham, 2020. Springer International Publishing.
- [88] Daniel Thomas. Deepfakes: A threat to democracy or just a bit of fun? *BBC News*, Jan. 2020.
- [89] Sergey Tulyakov, Ming-Yu Liu, Xiaodong Yang, and Jan Kautz. MoCoGAN: Decomposing Motion and Content for Video Generation. In *Proceedings of the IEEE Conference on Computer Vision and Pattern Recognition*, pages 1526–1535, 2018.
- [90] Junke Wang, Zuxuan Wu, Wenhao Ouyang, Xintong Han, Jingjing Chen, Yu-Gang Jiang, and Ser-Nam Li. M2TR: Multi-modal Multi-scale Transformers for Deepfake Detection. In *Proceedings of the 2022 International Conference on Multimedia Retrieval, ICMR '22*, pages 615–623, New York, NY, USA, June 2022. Association for Computing Machinery.
- [91] Yuxuan Wang, R.J. Skerry-Ryan, Daisy Stanton, Yonghui Wu, Ron J. Weiss, Navdeep Jaitly, Zongheng Yang, Ying Xiao, Zhifeng Chen, Samy Bengio, Quoc Le, Yannis Agiomyriannakis, Rob Clark, and Rif A. Saurous. Tacotron: Towards End-to-End Speech Synthesis. In *Interspeech 2017*, pages 4006–4010. ISCA, Aug. 2017.
- [92] Deressa Wodajo and Solomon Atnafu. Deepfake Video Detection Using Convolutional Vision Transformer, Mar. 2021. arXiv:2102.11126 [cs].
- [93] Mengmeng Xu, Chen Zhao, David S. Rojas, Ali Thabet, and Bernard Ghanem. G-TAD: Sub-Graph Localization for Temporal Action Detection. In *Proceedings of the IEEE/CVF Conference on Computer Vision and Pattern Recognition*, pages 10156–10165, 2020.
- [94] Ke Yang, Peng Qiao, Dongsheng Li, Shaohe Lv, and Yong Dou. Exploring Temporal Preservation Networks for Precise Temporal Action Localization. *Proceedings of the AAAI Conference on Artificial Intelligence*, 32(1), Apr. 2018. Number: 1.
- [95] Min Yang, Guo Chen, Yin-Dong Zheng, Tong Lu, and Limin Wang. BasicTAD: An astounding RGB-Only baseline for temporal action detection. *Computer Vision and Image Understanding*, 232:103692, July 2023.
- [96] Wenyuan Yang, Xiaoyu Zhou, Zhikai Chen, Bofei Guo, Zhongjie Ba, Zhihua Xia, Xiaochun Cao, and Kui Ren. AVoiD-DF: Audio-Visual Joint Learning for Detecting Deepfake. *IEEE Transactions on Information Forensics and Security*, 18:2015–2029, 2023. Conference Name: IEEE Transactions on Information Forensics and Security.
- [97] Xin Yang, Yuezun Li, and Siwei Lyu. Exposing Deep Fakes Using Inconsistent Head Poses. In *ICASSP 2019 - 2019 IEEE International Conference on Acoustics, Speech and Signal Processing (ICASSP)*, pages 8261–8265, May 2019. ISSN: 2379-190X.
- [98] Runhao Zeng, Wenbing Huang, Mingkui Tan, Yu Rong, Peilin Zhao, Junzhou Huang, and Chuang Gan. Graph Convolutional Networks for Temporal Action Localization. In *Proceedings of the IEEE/CVF International Conference on Computer Vision*, pages 7094–7103, 2019.
- [99] Chen-Lin Zhang, Jianxin Wu, and Yin Li. ActionFormer: Localizing Moments of Actions with Transformers. In Shai Avidan, Gabriel Brostow, Moustapha Cissé, Giovanni Maria Farinella, and Tal Hassner, editors, *Computer Vision – ECCV 2022*, Lecture Notes in Computer Science, pages 492–510, Cham, 2022. Springer Nature Switzerland.
- [100] Hang Zhao, Antonio Torralba, Lorenzo Torresani, and Zhicheng Yan. HACS: Human Action Clips and Segments Dataset for Recognition and Temporal Localization. In *Proceedings of the IEEE/CVF International Conference on Computer Vision*, pages 8668–8678, 2019.
- [101] Yue Zhao, Yuanjun Xiong, Limin Wang, Zhirong Wu, Xiaoou Tang, and Dahua Lin. Temporal Action Detection With Structured Segment Networks. In *Proceedings of the IEEE International Conference on Computer Vision*, pages 2914–2923, 2017.
- [102] Hang Zhou, Yasheng Sun, Wayne Wu, Chen Change Loy, Xiaogang Wang, and Ziwei Liu. Pose-Controllable Talking Face Generation by Implicitly Modularized Audio-Visual Representation. In *Proceedings of the IEEE/CVF Conference on Computer Vision and Pattern Recognition*, pages 4176–4186, 2021.
- [103] Tianfei Zhou, Wenguan Wang, Zhiyuan Liang, and Jianbing Shen. Face Forensics in the Wild. In *Proceedings of the IEEE/CVF Conference on Computer Vision and Pattern Recognition*, pages 5778–5788, 2021.
- [104] Yang Zhou, Xintong Han, Eli Shechtman, Jose Echevarria, Evangelos Kalogerakis, and Dingzeyu Li. MakeltTalk: speaker-aware talking-head animation. *ACM Transactions on Graphics*, 39(6):221:1–221:15, Nov. 2020.

- [105] Yizhe Zhu, Jialin Gao, and Xi Zhou. AVForensics: Audio-driven Deepfake Video Detection with Masking Strategy in Self-supervision. In *Proceedings of the 2023 ACM International Conference on Multimedia Retrieval, ICMR '23*, pages 162–171, New York, NY, USA, 2023. Association for Computing Machinery.
- [106] Bojia Zi, Minghao Chang, Jingjing Chen, Xingjun Ma, and Yu-Gang Jiang. WildDeepfake: A Challenging Real-World Dataset for Deepfake Detection. In *Proceedings of the 28th ACM International Conference on Multimedia, MM '20*, pages 2382–2390, New York, NY, USA, Oct. 2020. Association for Computing Machinery.